CHAPTER 2

Data and methods

RESULTS of astronomical research based on observations are hard to interpret even for experts without detailed knowledge about the data that was used and the way it was handled and analysed. A microlensing survey is not an exception. On the contrary, what kind of results can and will be obtained depends critically on the observational parameters and analysis techniques. In this chapter the data set used for the research in this thesis is described in section 2.1. Reduction and analysis are discussed in section 2.2.

2.1 Data acquisition

The Microlensing Exploration of the Galaxy and Andromeda has performed a microlensing survey in the direction of the Andromeda galaxy (M31). To obtain the best and most densely sampled lightcurves possible, several telescopes were used, the main ones being:
• Isaac Newton Telescope, Isaac Newton Group, La Palma
• Hiltner Telescope, MDM Observatory, Kitt Peak
• McGraw-Hill Telescope, MDM Observatory, Kitt Peak
• KPNO 4m Telescope, Kitt Peak National Observatory, Kitt Peak
This thesis concerns the analysis of data taken with the Isaac Newton Telescope (INT) on La Palma, although in chapter 5 they are complemented with data from the 4 meter Mayall telescope at the Kitt Peak National Observatory near Tucson Arizona. In this chapter the INT data set and the reduction and analysis methods will be described in detail.

Observations were carried out at two pointings in the Andromeda Galaxy, with the Wide Field Camera (WFC) of the INT. The WFC consists of four thinned EEV 2k×4k CCDs arranged as indicated in figure 2.1. With a pixel scale of $0.333''$ per pixel, the total area covered with these two pointings is approximately $0.5\ \mathrm{deg}^2$. The positions of the field centers and the layout of the fields, as shown in figure 2.1, were chosen such that good coverage of the minor axis of M31 was achieved, both on the far and the near side of the M31 disk. To increase the probability of detecting microlensing events due to the M31 dark halo, the far side of the disk is, however, covered more extensively than the near side.

Observations for the microlensing survey were carried out at the INT during four observ-

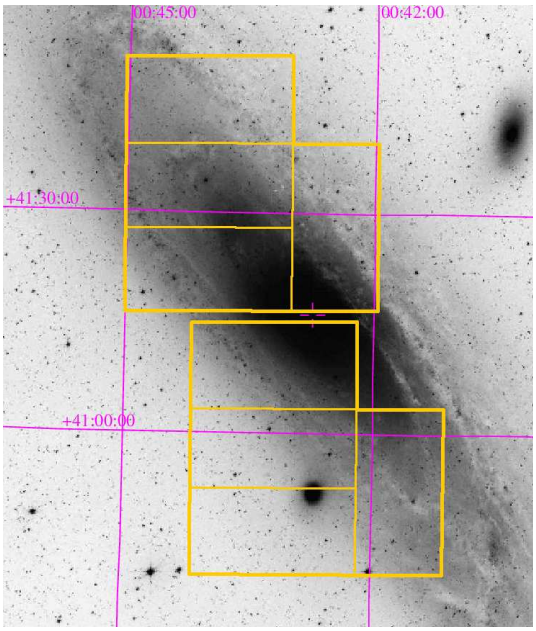

Figure 2.1 – the layout of the two INT Wide Field Camera (WFC) fields in M31 used for the microlensing search desribed in this thesis. The WFC has four 2048x4100 pixel chips, offering a field of view of approximately $0.25 \mathrm{deg}^2$. With this field layout we cover a large part of the far side of the disk of M31 as well as part of the near side.

ing seasons. These observing seasons extend from August to January, during which period M31 is best accessible from the northern hemisphere. The first observing season was August 1999 to January 2000 and the last August 2002 to January 2003. Since a dense time sampling is crucial for detecting microlensing the time was distributed as 1 or 2 hour allocations on all nights scheduled for use by United Kingdom or Netherlands observers during the 99B, 00B and 01B semesters. Since the WFC is not always mounted on the INT, observations tend to cluster in blocks of two to three weeks with comparable-sized gaps during which there are no observations. During the fourth observing season in semester 02B, 1 hour allocations were awarded on all nights scheduled for Netherlands observers and WFC Wide Field Survey (WFS) programs (Lewis et al. 1999). Observations were carried out for the most part by third party observers. Data were also obtained by INT staff during nights scheduled for engineering purposes or service-mode observing. To ensure a uniform dataset, fully automated scripts were used to do the observations during the last three seasons. For the first three seasons there was data-share agreement for the INT data with the POINT-AGAPE collaboration (Aurière et al. 2001).

For microlensing surveys it is important to use several filters, for a number of reasons. Information about the colour and colour change of a variable source can help distinguish microlensing events from variable stars. While variables usually change colour during the pulsations causing them to vary in brightness, microlensing events are achromatic and the relative change in flux is the same at all wavelengths. Furthermore, the colour of a microlensing event can help set constraints on the type of source star that is being lensed, and therefore on the initial flux of the source. The independent data sets also provide a way to test the reality of detected events.

During the first observing season three broad-band filters were used, namely g', r' and i'. These filters produce passbands that are similar to the Sloan Digital Sky Survey g', r' and i'

	r′		i′		g′	
	N	S	N	S	N	S
99/00	59	58	25	25	41	41
00/01	77	76	85	84	3	3
01/02	36	35	38	37	-	-
02/03	38	38	38	37	-	-
Total	210	207	186	183	44	44

Table 2.1 – Epochs obtained per season, for each filter and field.

bands. Most detectable microlensing events will have a Red Giant Branch star as their source star, due to their high brightness and large numbers. Because these stars have red colours, the use of the red r′ and i′ filters is advantageous. However, i′-band does suffer from fringing which affects the data quality. In the first season a mix of g′ and i′ images were obtained next to more extensive observations in r′. Because the fringing in i′-band was sufficiently weak for our purposes, in the second, third and fourth observing seasons, equal amounts of data were taken in r′ and i′-band.

For the analysis of the survey data, exposures of the same field with the same filter were combined per night. Each night therefore corresponds to one epoch in the survey and results in one point in the eventual lightcurves. Table 2.1 shows an overview of the number of epochs for which data was obtained during the INT survey for each filter and field. Clearly, in the first two seasons many more data were gathered than in the last two. The comparatively poor coverage in the third is due to weather conditions. Where in the first and second season respectively only 30% and 20% of the epochs were lost due to bad weather, as much as 60% of the epochs in the third season could not be obtained. During the fourth season weather did not play a big role, but the time allocation was smaller.

2.2 Data reduction and analysis

Standard data reduction, including bias subtraction, trimming, flatfielding and non-linearity correction was performed in IRAF. The same procedure was followed as used in the WFS reduction pipeline (Irwin & Lewis 2001), which also uses the WFC on the INT.

The conventional way of detecting microlensing events is by measuring the brightness of individual stars and looking for a temporary increase in the observed flux. In the case of microlensing of stars in the Andromeda galaxy (M31) this is not feasible. The reason is that because of the large distance to M31, the light of the stars is completely blended and individual stars can not be photometered, except for the extremely bright ones. For a microlensing survey in M31 a different technique is needed. The technique that was used for the work presented in this thesis is called Difference Image Photometry (DIP) and enables the detection of microlensing of unresolved stars.

In subsection 2.2.1 the principle of DIP is explained. After that the DIP pipeline used for the INT data is described in subsection 2.2.2.

2.2.1 Difference Image Photometry

At the basis of DIP lies a very simple idea, namely that of subtracting two images of the same field, taken at different times. Subtracting two identical images results in a 'difference

image' that is 'empty', whereas residuals will be left when the images are not identical. Crotts (1992) suggested that stellar variability in unresolved stellar fields in M31 might be measurable with this technique. Most stars are photometrically stable on timescales of a few years and therefore the subtracted images should have a smooth, zero mean background. Only at positions where stars vary in brightness, point source residuals will be left. In practice the procedure is not straightforward because changes in atmospheric conditions and telescope focus have to be corrected for. However, Gould (1996) showed that it is in principle possible to reduce the errors due to a time-variable PSF, photometric and geometric misalignment and discrete pixelization to below the photon noise.

The most complicated correction that has to be done before image subtraction is the correction for the changes in the PSF. Because of changing observing conditions and telescope focus imperfections the PSF is temporally variable, causing images taken some time apart to have different overall PSF. Especially for wide-field imagers, the PSF is also spatially variable over the focal plane. How the latter effect is handled is explained in section 2.2.2, here we concentrate on the general method of matching two different PSFs. The method used is based on Fourier convolution and was first used by Ciardullo et al. (1990) to search for novae in M31 globular clusters by subtracting frames taken in broad and narrow bands. Tomaney & Crotts (1996) showed that the method is very successful in detecting stellar variability in highly crowded fields in M31.

If the observed image would be a simple convolution of the actual image with the PSF, the actual image could in principle be obtained by deconvolution. But because of noise and pixelization effects, it is not possible to do this. Therefore, the only way to force the PSFs of two images to be the same, is by degrading the better seeing image and matching it's PSF to the PSF of the worse seeing image. Although degrading the image quality may seem undesirable, the PSF uniformity that can be obtained this way makes it possible to use image subtraction techniques.

Consider two images that have different PSFs, *r* and *i*, which can be related to each other by the convolution kernel *k*:

$$i = r * k. \tag{2.1}$$

According to the convolution theorem,

$$\mathcal{F}(i) = \mathcal{F}(r) \times \mathcal{F}(k) \tag{2.2}$$

where $\mathcal{F}$ is the Fourier transform. The kernel k can then also be represented by

$$k = \mathcal{F}^{-1}\left(\frac{\mathcal{F}(i)}{\mathcal{F}(r)}\right). \tag{2.3}$$

This means that in theory the convolution kernel can be determined from the PSFs of bright, unsaturated stars in the images. Of course one requirement is that the images are well sampled, at least with Nyquist sampling. In practice, however, the kernel k is sensitive to noise in the measured PSFs, which is a problem in the low signal-to-noise (S/N) wings of the PSF profiles. This problem is solved by replacing these wings with a 2-dimensional Gaussian below a certain threshold flux. Since the PSF usually is approximately a Gaussian, this approach works very well (e.g. Ciardullo et al. 1990; Tomaney & Crotts 1996; de Jong et al. 2004; Uglesich et al. 2004).

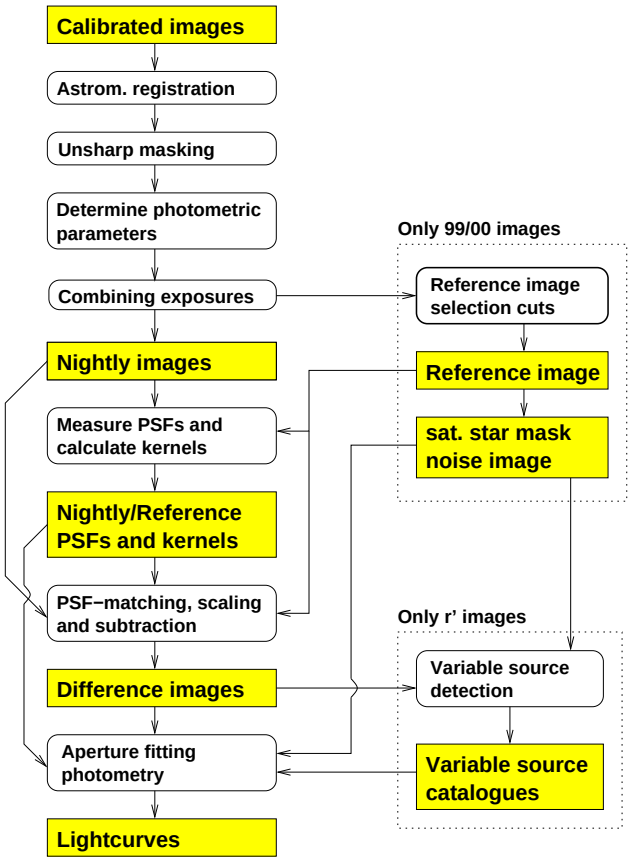

Figure 2.2 – Schematic overview of the DIP pipeline that was used to extract lightcurves of variable objects starting from the calibrated individual exposures. Parts of the process that involve only part of the total amount of data are indicated on the right of the main data flow. The shaded boxes indicate the important data files and the open boxes the important reduction steps.

2.2.2 Difference analysis pipeline

For the DIP analysis of the INT data a pipeline was developed, based on the DIFIMPHOT package for IRAF, written by Austin Tomaney. The pipeline starts after the standard calibration stage, described above, and produces lightcurves of variable sources in the surveyed fields. Although the WFC field is a mosaic of four CCDs, the analysis was done on a chip-per-chip basis, i.e. the chips were not combined into a mosaic. The pointing accuracy during the survey was good enough not to lose significant area using this strategy, as the gaps between the CCDs practically always cover the same area on the sky. Below follows a step-by-step description of the pipeline. In figure 2.2 a schematic overview of the pipeline is shown.

• *Astrometric registration*

The first step is the astrometric registration of all exposures to the same reference frame. For this purpose, an image with typical seeing and accurate pointing precision was chosen as the astrometric reference frame. In this image, sufficiently bright, unsaturated and isolated stars were detected to use for the astrometric registration. To ensure a good coverage of the whole CCD, the image area was divided in 16 (4×4) subregions, in each of which 15 stars were selected. In each individual exposure stars were detected in the same way and matched to

the stars in the astrometric reference image. The IRAF task GEOMAP was used to transform each exposure, using a third order polynomial with full cross-terms. Typically, the rms error of the registration was in the order of 0.03 pixels, increasing to around 0.1 pixels for frames with seeing greater than $2.0''$.

• *Unsharp masking*

Differences in the sky brightness need to be removed in order to make the high S/N reference image. However, subtraction of the sky level is not straightforward for our fields, since the smooth galaxy background is dominating everywhere. To circumvent this problem, all frames are "unsharp masked", i.e. a smoothed median background is subtracted from them. Because of the large amount of data we choose not to median average the full frames, but first block average the frames with 8×8 pixel blocks. The resulting 256×512 pixel sized image is then median averaged with a 7×7 pixel box size. After resizing the image to the original size, an 8×8 pixel boxcar smoothing is applied to smooth out pixelation. The thus obtained smoothed image is subtracted from the input frame, resulting in a zero-average image without sky or galaxy background. Both the smoothed background image and the unsharp masked image are kept, as also the background images are needed in some of the following steps. Some photometric parameters are measured on the unsharp masked images for the bright stars used for the astrometric registration. These photometric parameters will be used when combining the images into the reference and nightly stacks.

• *Reference image creation*

In order to measure flux changes of variable sources with respect to one common photometric standard, the same reference image has to be subtracted from all images. To minimize the noise in the resulting difference images, this reference image should have very high S/N. Creating such high S/N reference images is done by combining the best single exposures into stacked images. A further advantage of using stacked reference images is that they will be free of bad columns, cosmic rays and other defects. Exposures from the first (99/00) observing season were used to create the stacked reference images. To stack the exposures, they must first be photometrically scaled. For this, the photometric parameters of the list of bright, unsaturated stars that was used for the astrometric registration is used again. Scaling factors and FWHM are determined for all exposures. Possible variability of stars in the list might influence the determination of the scaling factors. Each star is checked for variability using all exposures with seeing better than 4 pixels ($1.33''$) and a list of constant stars is generated. A final determination of the photometric scaling factors is done with these constant stars. After this a weight is calculated for each image based on the photometric scaling factor and the seeing FWHM:

$$w = \frac{1}{FWHM^2 \times scale^2} \tag{2.4}$$

These weight factors are designed to maximise the S/N of faint objects in the final stacked reference frame.

After calculating the scaling factors and weights, all frames with a seeing FWHM smaller than 3.0 pixels ($1.0''$) and airmass smaller than 1.5 are selected. These are then photometrically scaled and combined through a weighted average. For some of the i' reference images the seeing criterium was loosened slightly to ensure a large enough number of exposures could be used. This was necessary because during the first season much less data was taken in i' than in r'. Typically between 10 and 20 exposures were combined to create the 8 r' reference images and between 6 and 10 exposures for the i' reference stacks. The combined

image has different noise charactaristics from the single exposures. To be able to determine meaningful errors during the photometry stage, these altered noise characteristics have to be determined. The effective gain G and read-noise R are calculated from the values g and r of the single exposures that went into the stack as follows:

$$G = \frac{\sum_i s_i g_i w_i}{\sum_i w_i}$$
$$R = \sqrt{\frac{\sum_i (s_i^2/g_i^2) r_i^2 w_i}{\sum_i w_i}} \tag{2.5}$$

These values are written into the headers of the reference images.

• *Auxiliary files creation*

Some more files that are needed further on in the pipeline are created based on the stacked reference image. Both when detecting variable sources in the difference images and when photometering them, bright stars and diffraction spikes can be a problem. Bright star masks are created based on the reference images that mask out all pixels with values higher than 6000 ADUs and all pixels within a 10 pixel radius of these. This cut at 6000 ADUs is necessary because some individual frames will have better seeing than the reference image which is a combination of several images. There is also a non-negligible non-linearity in the INT data that can cause problems in the subtraction of bright stars. This flux criterium takes care of almost all problematic areas, but a few more regions were added manually to the masks. These masks are later on used for all nightly difference images, both during variable source detection and during the photometry stage.

The main source of noise in the difference images will be due to photon noise. Since the photon noise scales with the square root of the signal, the parts of the field where the M31 background is high will be much noisier in the difference images. This can be a problem for the detection of variable sources in these bright parts of the field, but it can be counteracted by using a so-called noise image. The smoothed background image corresponding to the reference image is the combination of a large number of individual background images and is therefore practically noise-free and only contains the smoothed signal. From this stacked background image a noise image is made by taking the square root and multiplying by 2. When the difference images are divided by this noise image, the noise level becomes uniform.

• *Nightly images creation*

During observing nights usually at least two exposures were taken in every filter on every field. Per night the exposures are combined into one image in each filter of each field. For photometric scaling the parameters are used that were measured after the unsharp-masking step. Weights are calculated for the individual exposures in the same way as for the reference images. Exposures are then combined using the IRAF task IMCOMBINE with a weighted average and the "crreject" cosmic ray rejection, which compares pixel values with the expected noise from the CCD gain and read noise. The smoothed background frames are also combined. In some cases where the seeing differences between individual exposures were larger than $1''$, the PSFs of the frames were matched in the same way as is done before image subtraction before combining them. This especially was the case for nights in the first observing season when sometimes several exposures were taken at different times during the same night. The effective gain and read-noise are calculated according to equations 2.5 and written

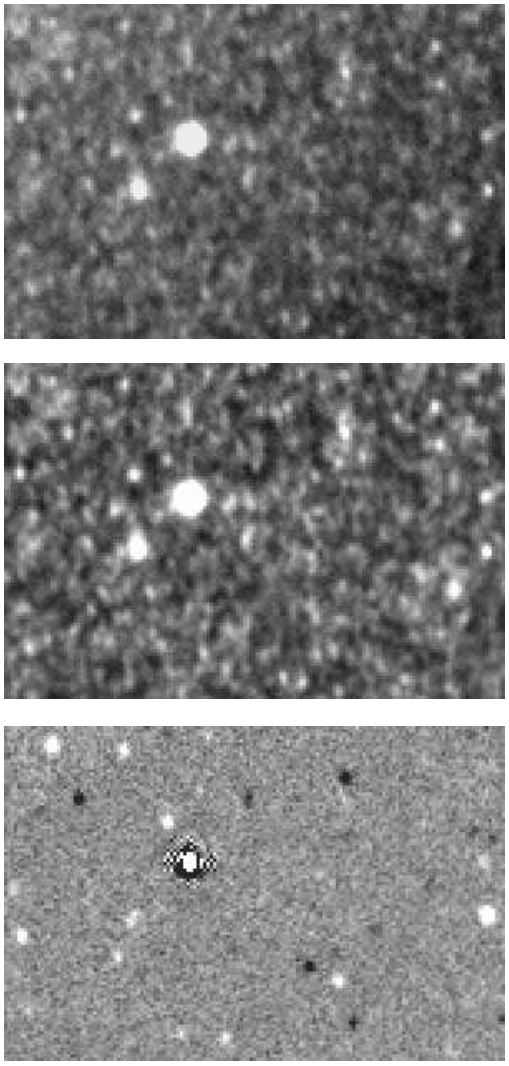

Figure 2.3 – Examples of what the images look like at different stages of the difference analysis pipeline. In the three panels the same $33'' \times 50''$ region is shown, located in the south field, approximately $8'$ from the bulge.
Upper panel: An individual calibrated exposure, as goes into the pipeline. This particular exposure was taken on December 31st 2002 and is in the r' filter.
Middle panel: After registration, unsharp-masking and combining two exposures the nightly image of December 31st 2002 looks like this. The slight galaxy background that can be seen in the calibrated exposure (getting brighter from the lower right to the upper left corner) is gone. The average pixel value of the nightly image is zero.
Lower panel: After photometric scaling, PSF-matching and subtraction of the reference image, this is what the difference image looks like. The background is dominated by photon noise. The bright, saturated star leaves a nasty residual and has to be masked during the variable source detection and also during the photometry stage. All the other positive (white) and negative (black) residuals are due to sources that are respectively brighter or fainter in the nightly image than in the reference image.

to the image headers. Since all exposures are combined per night for all further analysis, we will consider every night for which combined images are available as an epoch.

• *PSF measurement, matching kernel generation*
To derive the PSF matching kernels, the PSFs of the reference images and the nightly images must be measured. As mentioned before, the PSF is not only varying temporally but also spatially. To cope with this problem, each image will be divided into 16 (4×4) subregions for each of which separate matching kernels will be calculated. This means that for each image the PSF is determined for each of these 16 regions. The stars in the list of constant, bright stars obtained in the previous step are used for this purpose. A 25×25 pixel region is extracted around every star. Because of the crowding in the M31 fields it is best to use a large

number of stars to get a clean PSF, so for every region at least 15 stars are demanded. The original list of stars used for astrometric registration contained 15 stars per subregion, but in some cases up to half of them were removed because of variability, so in the case a subregion does not contain enough constant, bright stars, nearby stars from surrounding subregions are added until 15 stars are selected. After subtracting any left over sky, the stellar images are normalised. Then the postage stamps are combined using an algorithm that looks a bit like a median, but instead rejects the 6 highest and lowest pixel values and takes the average of the 3 remaining pixel values. The thus obtained, normalised PSFs will be used for the PSF-fitting photometry and for deriving the PSF matching kernels.
How the matching kernels can be derived from the PSFs was described in section 2.2.1 and the IRAF routine PSFMATCH (Phillips & Davis 1995) is used to do these steps. These steps involve taking the Fourier transform of the PSFs of the subregions in each nightly image and the reference image, taking the ratios, fitting the low S/N wings of the result with an elliptical gaussian and finally taking the Fourier transform of the result, which then are the matching kernels. In most cases the reference image will be the image that has to be degraded in seeing, but sometimes the nightly image will have the better seeing.

• *Photometric scaling and subtraction*
With the matching kernels available, subtraction is almost possible. For each epoch, either the nightly image or the reference image is PSF-matched to the worse seeing image, subregion by subregion. Again, the PSFMATCH task is used for this. Using the list of bright, constant stars, the photometric scaling factor between the matched images is determined and the nightly image is photometrically scaled to match the reference image, irrespective of which image was degraded. Finally, the reference image is subtracted from the nightly image. What is left after subtraction are the so-called difference images, which if everything went well, should have a background of photon noise with residuals where objects changed in brightness. In the case of our M31 fields this means there are positive of negative point source residuals caused by stellar variability. Updated values of the effective gain and read-noise for the difference images are calculated, taking into account all the scaling and convolution steps. Examples of part of an individual exposure, a stacked nightly image and a difference image are shown in figure 2.3.

• *Variable source detection*
In principle, variables sources can be detected rather easily in the difference images. Before finding the residuals, the high noise levels in bright parts of the field have to be dealt with. All difference images are divided through the noise images that were created from the high S/N smoothed background images created together with the reference images, leaving difference images with uniform noise backgrounds.
The SExtractor program (Bertin & Arnouts 1996) is used to do the residual detection. Advantages of this program are the fact that it determines the background and standard deviation locally and looks for groups of connected pixels that are at least a specified amount above the local background. We search all difference images for both positive and negative residuals that have at least 4 pixels that are at least 3σ above the background. Since SExtractor does not deal with negative sources, the difference images have to be inversed to find these.
Some cleaning of the source lists is necessary. SExtractor flags objects that show certain problems, like containing pixel values above a specified saturation level, enabling us to filter out detections in or too close to the masked regions. Due to slight offsets in pointing, some difference images contain regions near the edges that can not be used. After cleaning the

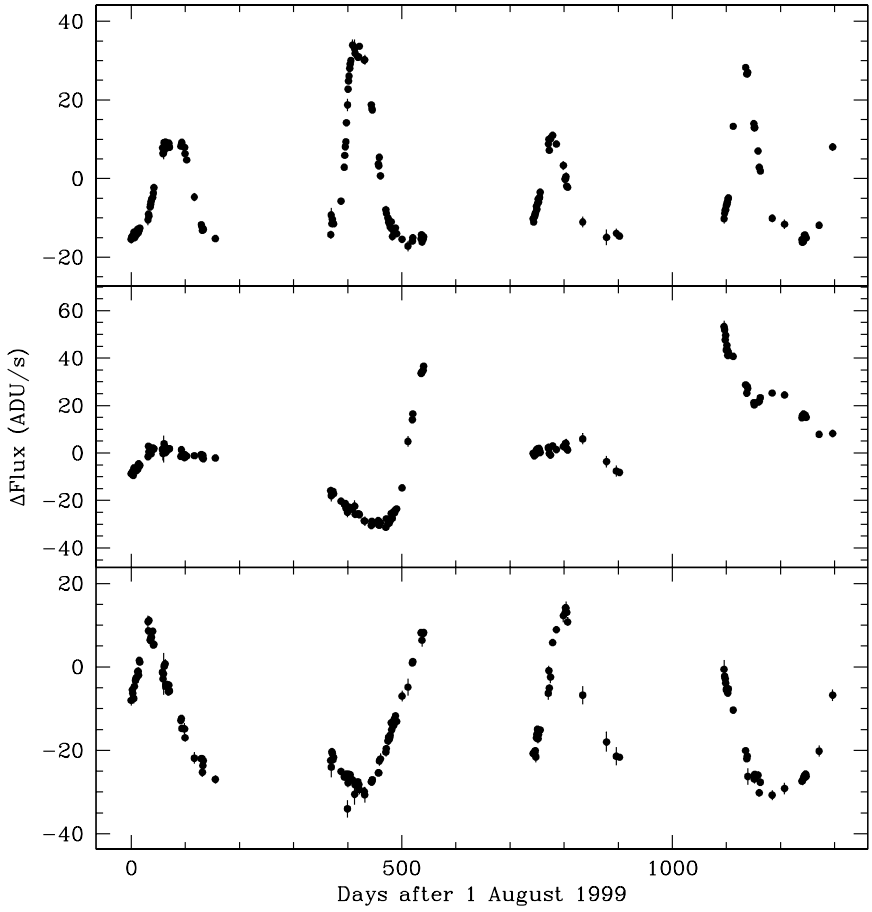

Figure 2.4 – Three lightcurves of variable stars obtained with the difference image analysis described in this section. Almost all variable objects that are detected in M31 are variable stars.

individual source lists, they are combined into master catalogues per chip. To remove spurious detections, only variable sources are retained that were detected in at least 2 difference images.

• *Aperture fitting photometry*

Once all detected variable sources are collected in master catalogues, they can be photometered to create lightcurves. The photometry for the lightcurves presented in chapter 3 was done in slightly different way than for the lightcurves presented in the other chapters. However, the basic method is the same and is described here.

PSF-fitting photometry is done on the residuals in the difference images within a certain

aperture, the extraction aperture. This is done using an optimal extraction algorithm (Naylor 1998) that replaces pixels deviating more than a specified number of σ with the model PSF. For each subregion in each difference image the PSF is used that was used to create that specific part of the difference image, i.e. either the local PSF of the reference image or the local PSF of the corresponding nightly image. The photometry routine then outputs the fitted flux within the extraction aperture. The size of the extraction aperture is specified in terms of the FWHM of the PSF, so that for every epoch the same ratio of the total flux in the residual is measured. For the analysis in chapter 3 an extraction aperture with radius 1.5 FWHM was used. Because, especially in i′, in some parts of the field the residuals start to get crowded, a smaller aperture of 0.5 FWHM was used in chapters 4, 5 and 6.

The shape of the PSFs is not perfectly gaussian and varies between difference images. This means that even when scaling the extraction aperture with the FWHM, the ratio of the total flux that is measured is not always the same. This is corrected for by comparing the flux within the extraction aperture with the flux within a large normalisation aperture, radius 3 FWHM, which contains most of the flux. This ratio is determined for all local PSFs. The flux measured for a residual within the extraction aperture is multiplied by this ratio and divided by the same ratio measured for the corresponding local PSF of the reference image. In this way the flux corresponds to the flux within the extraction aperture for the PSF shape of the reference image. With this PSF shape the total flux in the residual can be calculated for all epochs using the reference images PSFs.

Standard deviations for the measured fluxes include the photon noise and the error in the photometric scaling of the nightly image to the reference image. For the determination of the photon noise, the smoothed background for each background image is added to the difference image. The local sky background is then determined in a ring around the residual, of which the inner radius and width scale with the FWHM. To check the error bars, in every chip around 1500 lightcurves were produced at positions where no variable sources are located. Constant line fits were done to these lightcurves and for each epoch the distribution of the deviations from these fits weighted by the error bars was examined. If the error bars are correct, this distribution should be a gaussian with dispersion 1. For epochs where this distribution had a dispersion higher than one, the error bars were scaled up appropriately.

This concludes the discussion of the difference imaging pipeline. At this point the lightcurves are ready for further analysis. In figure 2.4 three examples of lightcurves delivered by the pipeline are shown. Further analysis of the database of lightcurves is discussed in detail in the following chapters.